Journal of Power Sources 246 (2014) 124–131

Contents lists available at ScienceDirect

Journal of Power Sources

journal homepage: www.elsevier.com/locate/jpowsour

Three-dimensional-network $Li_3V_2(PO_4)_3$/C composite as high rate lithium ion battery cathode material and its compatibility with ionic liquid electrolytes

Jiantie Xu [a], Shu-Lei Chou [a,*], Cuifeng Zhou [b], Qin-Fen Gu [c], Hua-Kun Liu [a], Shi-Xue Dou [a]

[a] Institute for Superconducting and Electronic Materials, University of Wollongong, Wollongong, NSW 2522, Australia
[b] Australian Centre for Microscopy and Microanalysis, The University of Sydney, NSW 2006, Australia
[c] Australian Synchrotron, 800 Blackburn Rd, Clayton 3168, Australia

HIGHLIGHTS

- Microwave-assisted hydrothermal synthesis of $Li_3V_2(PO_4)_3$/C.
- $Li_3V_2(PO_4)_3$/C shows 3D network structure with nanowires and microsized particles.
- High rate and long life: 103.4 mAh g^{-1} at 10C after 500 cycles.
- Compatibility of $Li_3V_2(PO_4)_3$/C with ionic liquid electrolytes.

ARTICLE INFO

Article history:
Received 3 June 2013
Received in revised form
4 July 2013
Accepted 10 July 2013
Available online 26 July 2013

Keywords:
Lithium ion battery
Cathode materials
$Li_3V_2(PO_4)_3$
Microwave-assisted hydrothermal method
Ionic liquids

ABSTRACT

A high performance $Li_3V_2(PO_4)_3$ cathode material for lithium ion batteries was synthesized by the microwave-assisted hydrothermal method followed by a post annealing process. The synchrotron X-ray diffraction analysis results confirmed that single-phase $Li_3V_2(PO_4)_3$ with monoclinic structure was obtained. Scanning electron microscope and transmission electron microscope images revealed that the as-prepared $Li_3V_2(PO_4)_3$ was composed of nanowires and microsized particles. Electrochemical results demonstrated that the $Li_3V_2(PO_4)_3$ electrode measured at 10 C after 500 cycles can deliver discharge capacities of 85.4 mAh g^{-1} and 103.4 mAh g^{-1}, with a capacity retention of 99.3% and 95.9%, in the voltage ranges of 3.0–4.3 V and 3.0–4.8 V, respectively, indicating good cycling stability. Furthermore, the electrochemical performance of $Li_3V_2(PO_4)_3$ in ionic liquid electrolytes between 3.0 V and 4.8 V was also measured.

1. Introduction

Since $LiFePO_4$ was proposed as a cathode material for the lithium ion battery by Goodenough et al. [1] in 1997, it has been widely viewed as one of the most promising candidates for large-scale commercialization because of its high capacity, thermal stability, environmental benignity, and low cost. Other lithium transition metal phosphates, including $LiMPO_4$ (M = Mn, Co, Ni) [2,3], $Li_3V_2(PO_4)_3$ [4,5], $LiVOPO_4$ [6,7], $Li_9M_3(PO_4)_2(P_2O_7)_3$ (M = V, Cr, Al, Ga) [8,9], $Li_2MP_2O_7$ (M = Mn, Co, Fe) [10,11], and their derivatives [12–14], have also received considerable attention due to their great thermal stability and competitive energy density. Compared to $LiFePO_4$, one in particular, $Li_3V_2(PO_4)_3$, shows higher theoretical capacity (~197 mAh g^{-1} vs. ~170 mAh g^{-1} for $LiFePO_4$) and a higher average operation voltage plateau (~4.0 V vs. ~3.3 V for $LiFePO_4$), leading to higher energy density (~800 Wh g^{-1} vs. ~560 Wh g^{-1} for $LiFePO_4$). Nevertheless, the low intrinsic electronic conductivity (~2.4×10^{-7} S cm^{-1}), high working potential (up to 4.8 V), and low Li^+ diffusion coefficient (10^{-10}–10^{-9} cm^2 s^{-1}) of $Li_3V_2(PO_4)_3$ lead to a poor high rate performance and unstable electrolyte, which thus limit its practical application [15]. To improve the high rate capabilities of $Li_3V_2(PO_4)_3$, there have been a few reports on $Li_3V_2(PO_4)_3$ morphology control, such as the synthesis of nanofibers [16], nanorods [17], nanoplates [18], nanobelts [19], and nanoporous material [20,21] through various preparation methods, and those nanostructures are proved to be an effective

* Corresponding author.
E-mail addresses: shulei@uow.edu.au, sc478@uow.edu.au (S.-L. Chou).

0378-7753/$ – see front matter © 2013 Elsevier B.V. All rights reserved.
http://dx.doi.org/10.1016/j.jpowsour.2013.07.055

way to improve the high rate capabilities of electrode materials. The large amount of nanosize materials with high surface area, however, will reduce the volumetric energy density of lithium ion batteries and aggravate the side reaction between the active materials and the electrolyte. Therefore, an electrode material with micrometer-sized particles composed of nanometer-sized particles is an ideal morphology to effectively improve both volumetric energy density and rate capability [22].

Furthermore, to reach the high theoretical specific capacity (~197 mAh g^{-1}), the $Li_3V_2(PO_4)_3$ electrode must be fully charged to ~4.8 V ($V^{3+} \rightarrow V^{5+}$). Conventional electrolytes ($LiPF_6$ in ethylene carbonate: diethyl carbonate (EC: DEC) or EC: dimethyl carbonate (DMC)), however, will decompose at such a high voltage (>4.6 V). The electrolyte decomposition will severely increase the explosion and fire risk of lithium ion batteries. Ionic liquids (ILs), on the other hand, have been receiving greater attention in the lithium ion battery field because of their non-flammability, negligible vapour pressure, and high thermal, chemical, and electrochemical stability. Among the large family of ILs, pyrrolidinium bis(trifluoromethane sulfonyl) amide salts in particular show high cathodic stability against lithium metal, relatively high ionic conductivity, non-flammability, and also good electrochemical properties in battery tests [23–25].

The microwave-assisted hydrothermal method could be employed to prepare $Li_3V_2(PO_4)_3$ because it combines the advantages of the hydrothermal method [17,18,26–29] and the microwave assisted method [30,31], including morphology control, low cost, short reaction time, and high efficiency. Here, we have successfully adopted a new synthesis route based on the micro wave-assisted hydrothermal method to obtain a three-dimen sional (3D) $Li_3V_2(PO_4)_3$/C microsize network morphology. The electrochemical performances of $Li_3V_2(PO_4)_3$ measured in conventional electrolyte and in ILs are also compared.

2. Experimental section

A schematic representation of the preparation of the 3D $Li_3V_2(PO_4)_3$/C nanowire and nanoparticle network morphology is presented in Fig. 1(a). 0.0075 mol lithium acetate hydrate ($CH_3COOLi \cdot 2H_2O$), 0.005 mol ammonium metavanadate (NH_4VO_3), and 0.0075 mol ammonium dihydrogen phosphate ($NH_4H_2PO_4$) were dissolved in 20 mL distilled water to form a solution. 0.228 g glucose and 1 mL of ethylene glycol (EG) were then added to the solution. The solution was stirred for 2 min before being transferred into a 100 mL Teflon-lined microwave vessel. The microwave vessel was sealed, kept at 180 °C for 15 min in a microwave oven, and then cooled to room temperature naturally. After that, the solution with its black suspension was heated under continuous stirring in a 80 °C thermostatic water bath for several hours to remove the excess water. Finally, the powder was annealed at 750 °C for 10 h, with a heating rate of 5 °C min^{-1} under high purity Ar atmosphere, and then naturally cooled down to room temperature under the same Ar atmosphere.

Synchrotron powder X-ray diffraction (SXRD) data for Rietveld analysis was collected at a room temperature over the range of 3°–86° with a Mythen detector on the Powder Diffraction Beamline at the Australian Synchrotron (Melbourne, Australia). Rietveld refinement was performed using GSAS software [32]. The morphology of the $Li_3V_2(PO_4)_3$/C was examined with a high resolution field emission scanning electron microscope (SEM; JEO: FESEM-7500, 30 kV) and a transmission electron microscope (TEM; JEO: 2200FS, 200 kV). The carbon content of the $Li_3V_2(PO_4)_3$/C was obtained by thermogravimetric analysis (TGA, Mettler Toledo). The specific surface area, 11.9 m^2 g^{-1}, was measured by the Brunauer–Emmett–Teller (BET) method on a Quanta Chrome Nova 1000.

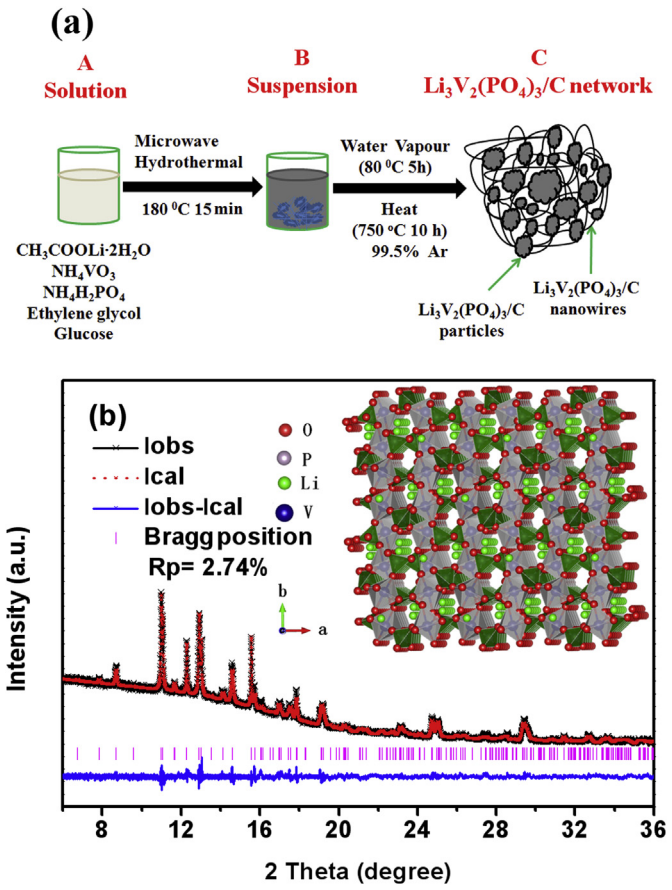

Fig. 1. (a) Schematic representation of formation mechanism of 3D $Li_3V_2(PO_4)_3$ nanowire and nanoparticle network system. (b) SXRD Rietveld refinement of $Li_3V_2(PO_4)_3$, where the observed data are indicated by the black symbols and the calculated profile is the red dotted line overlaying them. The lower curve is the difference between the observed and calculated intensities at each step, plotted on the same scale and shifted a little downwards for clarity. Inset of Fig. 1(b): the crystal structure of $Li_3V_2(PO_4)_3$ based on the SXRD refinement. (For interpretation of the references to colour in this figure legend, the reader is referred to the web version of this article.)

The cathodes were fabricated by blending the $Li_3V_2(PO_4)_3$/C with acetylene black carbon and poly(vinylidene difluoride (PVDF)), at a weight ratio of 8:1:1, respectively. N-Methyl-2-pyrrolidone (NMP) was used as the blending solvent for the mixture. The slurries were prepared using a Kurabo MAZERUSTAR planetary mixer (KK-250S, Kurabo Industries Ltd., Japan) for 15 min. The obtained slurry was coated on Al foil, dried at 90 °C for 12 h, and pressed at a pressure of 2 MPa. After fabrication, the electrodes were dried again at 90 °C for 12 h in a vacuum after cutting them into a 1 cm × 1 cm size, with a loading of about 7 mg of active materials. CR 2032 coin-type cells were assembled using $Li_3V_2(PO_4)_3$/C as the working electrode, Li foil as the counter electrode and reference electrode, porous polypropylene film as a separator, and 1 M $LiPF_6$ (Sigma–Aldrich) in a 1:2 (v/v) mixture of ethylene carbonate (EC) (Sigma–Aldrich) and diethyl carbonate (DEC) (Sigma–Aldrich), or 1 M lithium bis(trifluoromethane sulfonyl)imide ($LiNTf_2$) (Sigma–Aldrich) in N-butyl-N-methyl-pyrrolidinium bis(trifluoromethanesulfonyl)imide ([C_4mpyr][NTf_2]) (TCI America) ionic liquid, or 1 M lithium bis(trifluoromethane sulfonyl)imide ($LiNTf_2$) (Sigma–Aldrich) in N-methyl-N-propylpyrrolidinium bis(trifluoromethanesulfonyl)imide ([C_3mpyr][NTf_2]) (TCI America) ionic liquid as the three different kinds of electrolyte. The cells were measured using a battery testing system

(Land®, China) and galvanostatically charged and discharged at various current densities in the voltage ranges of 3.0–4.3 or 3.0–4.8 V, with 1C = 197 mAh g^{-1} for both voltage ranges. Cyclic voltammetry was conducted using a Biologic VPM3 electrochemical workstation.

3. Results and discussion

Since small amounts of impurities affect the electrochemical properties, the precise XRD pattern is important for obtaining the details of the crystal structure. Fig. 1(b) shows the Rietveld refinement results of the synchrotron powder X-ray diffraction (SXRD) data for $Li_3V_2(PO_4)_3$/C compound sintered at 750 °C, with space group $P2_1/n$ chosen as the refinement model. The reasonably small agreement factors, R_p (2.74%) and R_{wp} (4.01%), suggest that single-phase $Li_3V_2(PO_4)_3$/C can be obtained in our experimental process. The cell parameters are a = 8.6291(8) Å, b = 12.0818(6) Å, c = 8.6414(2) Å, β = 90.022(1)°, and the unit-cell volume is 900.927(3) $Å^3$. The cell parameters are consistent with previous reports [33–36].

The SEM image of $Li_3V_2(PO_4)_3$/C in Fig. 2(a) shows that the bulk $Li_3V_2(PO_4)_3$/C is made up of agglomerated, uniform microsized particles. Nanowires ~50 nm in diameter and big particles can be seen in Fig. 2(b). Moreover, transmission electron microscopy (TEM) and energy dispersive X-ray spectroscopy (EDS) were conducted to further confirm the microstructure of $Li_3V_2(PO_4)_3$/C. As shown in Fig. 2(c) and (d), the selected areas all exhibit the characteristic peaks of V, P, C, and O in the sample. The intensities of the peaks are related to the contents of the different elements, as we selected spots for analysis without the carbon covering on the TEM grid for both the $Li_3V_2(PO_4)_3$ particles and the nanowires. The nanowires show a much higher intensity carbon peak than the particles, indicating much higher carbon content in the nanowire structure. High resolution TEM (HRTEM) and Fourier transform

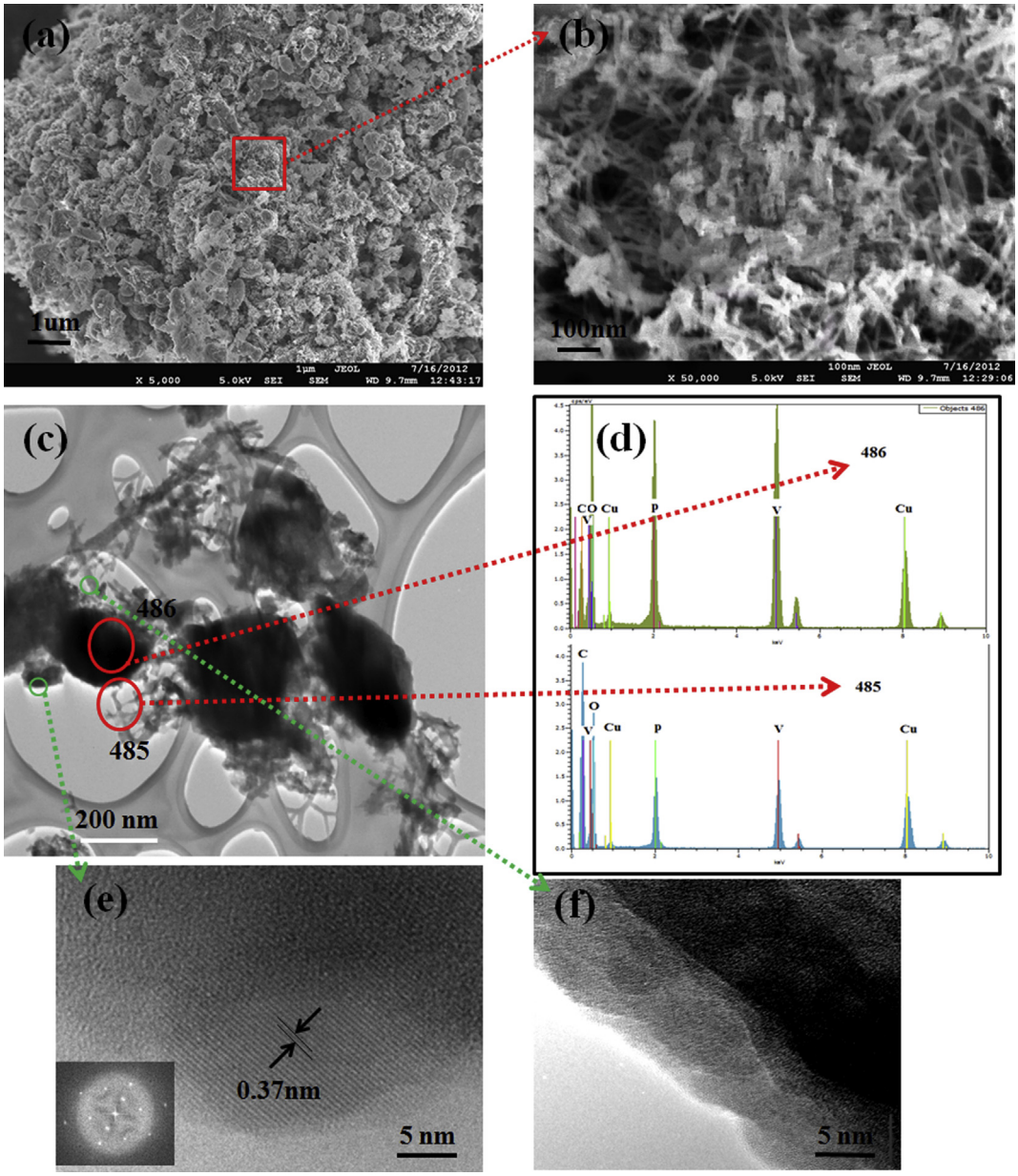

Fig. 2. (a, b) SEM and (c) TEM images of $Li_3V_2(PO_4)_3$/C; and (d) EDS spectra corresponding to the circled areas in (d); (e, f) corresponding HRTEM images from the marked regions showing the single-crystalline structure. Inset of (e): corresponding Fourier transform image.

images of a $Li_3V_2(PO_4)_3$/C particle are shown in Fig. 2(e). The particle is well crystallized and has a small amount of amorphous carbon coating. The HRTEM image shown in Fig. 2(f) indicates that the nanowires of the $Li_3V_2(PO_4)_3$/C sample contain large amounts of carbon, which provides the 3D conducting matrix to improve the electron transport along the nanowires. At the same time, the crystallized $Li_3V_2(PO_4)_3$/C particles are acting as the host of the lithium ions. Sun et al. [26] showed that there were agglomerated particles of $Li_3V_2(PO_4)_3$/C when glucose was added before hydrothermal treatment. Zhu et al. [37] suggested that glucose not only facilitates the formation of FeOOH nanorods, but also gives rise to a uniform, glucose-derived, carbon-rich polysaccharide (GCP) overlayer on the FeOOH nanorods. Therefore, we suggest that the glucose plays the key role in the $Li_3V_2(PO_4)_3$/C nanowire formation during microwave-assisted hydrothermal treatment.

As shown in Fig. 3, thermogravimetric analysis (TGA) was adopted to estimate the amorphous carbon content in the $Li_3V_2(PO_4)_3$/C. The individual causes of the total mass changes (Δm) can be determined from room temperature to 900 °C: evaporation of moisture (m_w), gasification of carbon (m_c), and oxidation of $Li_3V_2(PO_4)_3$/C (m_o), namely:

$$\Delta m = -m_w - m_c + m_o \quad (1)$$

$$\Delta m = -m_w - m_c + k(1 - m_c - m_w) \quad (2)$$

Where $m_w = \sim 0.43\%$, $\Delta m = \sim 0.27\%$, and the oxidation coefficient ($k = 0.0784$) was obtained from the Kuang et al. [38] results on $Li_3V_2(PO_4)_3$/C oxidation over the temperature range of 50–900 °C. Based on Equations (1) and (2), $m_c = 6.74\%$.

Fig. 4(a, b) shows typical charge/discharge profiles of $Li_3V_2(PO_4)_3$/C in the voltage ranges of 3.0–4.3 V and 3.0–4.8 V, respectively, at various current rates. As shown in Fig. 4(a, b), the curves for $Li_{3-x}V_2(PO_4)_3$/C maintain flatter charge–discharge plateaus in the voltage range of 3.0–4.3 V at different current densities than those in the voltage range of 3.0–4.8 V because of the more stable $Li_{3-x}V_2(PO_4)_3$ ($x = 0$–2) structure during the extraction–insertion. The plateau boundaries of $Li_{3-x}V_2(PO_4)_3$ ($x = 0$–3) become ambiguous or disappear in the charge/discharge curves, due to the disordering of Li ions during the extraction–insertion after fully charging to 4.8 V ($x = 2 \rightarrow 3$). Moreover, with increased charging/discharging current densities, these plateaus become shorter, and the difference in potential (ΔV) between the charging and discharging plateaus increases gradually, because of the electrode polarization at high C-rates. The differential capacity vs. voltage (dQ/dV) curves for $Li_3V_2(PO_4)_3$/C in the voltage ranges of 3.0–4.3 V and 3.0–4.8 V are shown in Fig. 4(c, d), respectively. $Li_3V_2(PO_4)_3$/C presents three pairs of oxidation and reduction peaks in the voltage range of 3.0–4.3 V, while four oxidation peaks and three reduction peaks are observed in the voltage range of 3.0–4.8 V, corresponding to the relevant extraction–insertion of Li^+. For example, if the cell is charged to 4.8 V, all three Li^+ ions are extracted from monoclinic $Li_3V_2(PO_4)_3$ over four two-phase electrochemical plateaus at 3.60 V, 3.68 V, 4.08 V, 4.53 V during the charge process, which correspond to different phases of $Li_xV_2(PO_4)_3$ at $x = 3.0$, 2.5, 2.0, 1.0, 0.5, respectively. Three plateaus at 4.03 V, 3.65 V, 3.57 V are observed during the discharge process, which correspond to different phases of $Li_xV_2(PO_4)_3$ at $x = 2.0$, 1.0, 0.5, respectively. This electrochemical behaviour agrees well with previous results [18,35,36,39]. Moreover, as shown in Fig. 4(c, d), the specific energy density has also been estimated for both voltage ranges by using the area integrals of the initial charge–discharge curves (Fig. 4(a, b)) at each different plateau region.

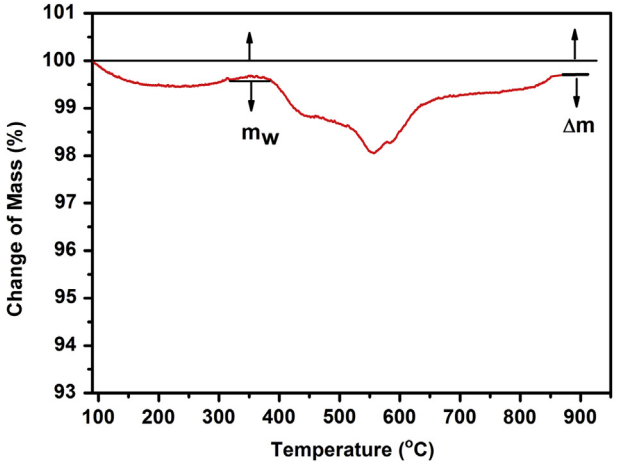

Fig. 3. TGA curve for $Li_3V_2(PO_4)_3$/C.

In order to investigate the rate and cycling performance of $Li_3V_2(PO_4)_3$/C, the $Li_3V_2(PO_4)_3$/C cells were charged and discharged for 120 cycles in the voltage ranges of 3.0–4.3 V and 3.0–4.8 V, respectively, at various current rates. As shown in Fig. 5(a), the first cycle discharge capacity in the voltage range of 3.0–4.3 V of $Li_3V_2(PO_4)_3$/C at 0.1C was 128.5 mAh g^{-1}, while the discharge capacity of 162.7 mAh g^{-1} was delivered by the $Li_3V_2(PO_4)_3$/C in the voltage range of 3.0–4.8 V at 0.1C in the first cycle. At 20 C, the capacity retention of $Li_3V_2(PO4)_3$/C in the voltage ranges of 3.0–4.3 V and 3.0–4.8 V is 36.2% and 52.9% of initial capacity, respectively. The higher capacity retention in the voltage range of 3.0–4.8 is probably attributable to the strong electrolyte decomposition and the formation of solid electrolyte interphase (SEI). In Fig. 5(c, d), the relatively long-term cycling performance and the coulombic efficiency for $Li_3V_2(PO_4)_3$/C are compared at 10 C for the voltage ranges of 3.0–4.3 V and 3.0–4.8 V. It can be found from Fig. 5(c) that the $Li_3V_2(PO_4)_3$/C has an initial discharge capacity of 86 mAh g^{-1} and 107.8 mAh g^{-1} at 10 C in the voltage ranges of 3.0–4.3 V and 3.0–4.8 V, respectively. Even after 500 cycles, the $Li_3V_2(PO_4)_3$/C cells can still deliver discharge capacities of 85.4 mAh g^{-1} and 103.4 mAh g^{-1}, with capacity retention compared to initial capacity of 99.3% and 95.9%, for the 3.0–4.3 V and 3.0–4.8 V voltage ranges, respectively, indicating the good cycling performance for both voltage ranges. The $Li_3V_2(PO_4)_3$/C electrodes measured in the voltage ranges of 3.0–4.3 V and 3.0–4.8 V, however, both present high average coulombic efficiency, approaching 99.5% at 10C (Fig. 5(d)), indicating that the $Li_3V_2(PO_4)_3$/C has an excellent stable structure. The good high rate cycling performance and high coulombic efficiency could be attributed to the 3D network structure of the $Li_3V_2(PO_4)_3$/C, which could effectively facilitate lithium ion extraction and insertion, leading to the very good high rate capacity. The long-term cycling stability at high rate of this $Li_3V_2(PO_4)_3$/C compound is comparable to or even much better than those in previous reports that were synthesized by the hydrothermal method alone [17,18,26–29] or the microwave assisted method alone [30,31]. For example, Liu et al. [17] reported that nanorod-like $Li_3V_2(PO_4)_3$ gave a discharge capacity of 101.1 mAh g^{-1} at 10 C (1C = 180 mAh g^{-1}) in the voltage range of 3.0–4.6 V, but there were no results on long term cycling performance for their $Li_3V_2(PO_4)_3$ (only 5 cycles). Qiao et al. [18] found that plate-like $Li_3V_2(PO_4)_3$ showed a discharge capacity of 111.8 mAh g^{-1} at 3C in the voltage range of 3.0–4.8 V with 66.0% capacity retention after 500 cycles. Sun et al. [26] reported that the reversible specific capacity of $Li_3V_2(PO_4)_3$ was 60 mAh g^{-1} at 5 C in the voltage range of 3.0–4.8 V. Yan et al. [31] employed a fast sol–gel assisted microwave heating approach to prepare $Li_3V_2(PO_4)_3$/C, with the particle

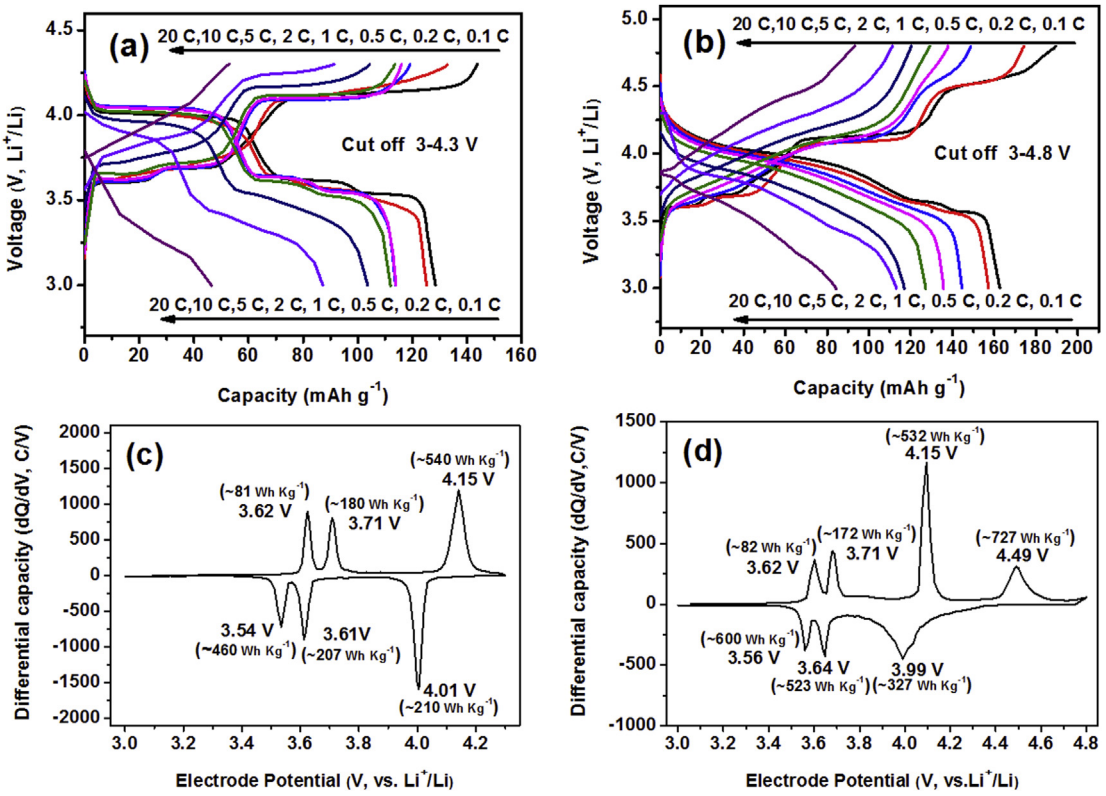

Fig. 4. Initial charge–discharge curves (a, b) and d*Q*/d*V* (c, d) for $Li_3V_2(PO_4)_3$/C in the voltage ranges of 3.0–4.3 V (a, c) and 3.0–4.8 V (b, d) (1 M $LiPF_6$ in a 1:2 (v/v) mixture of ethylene carbonate (EC) and diethyl carbonate (DEC) as the electrolyte).

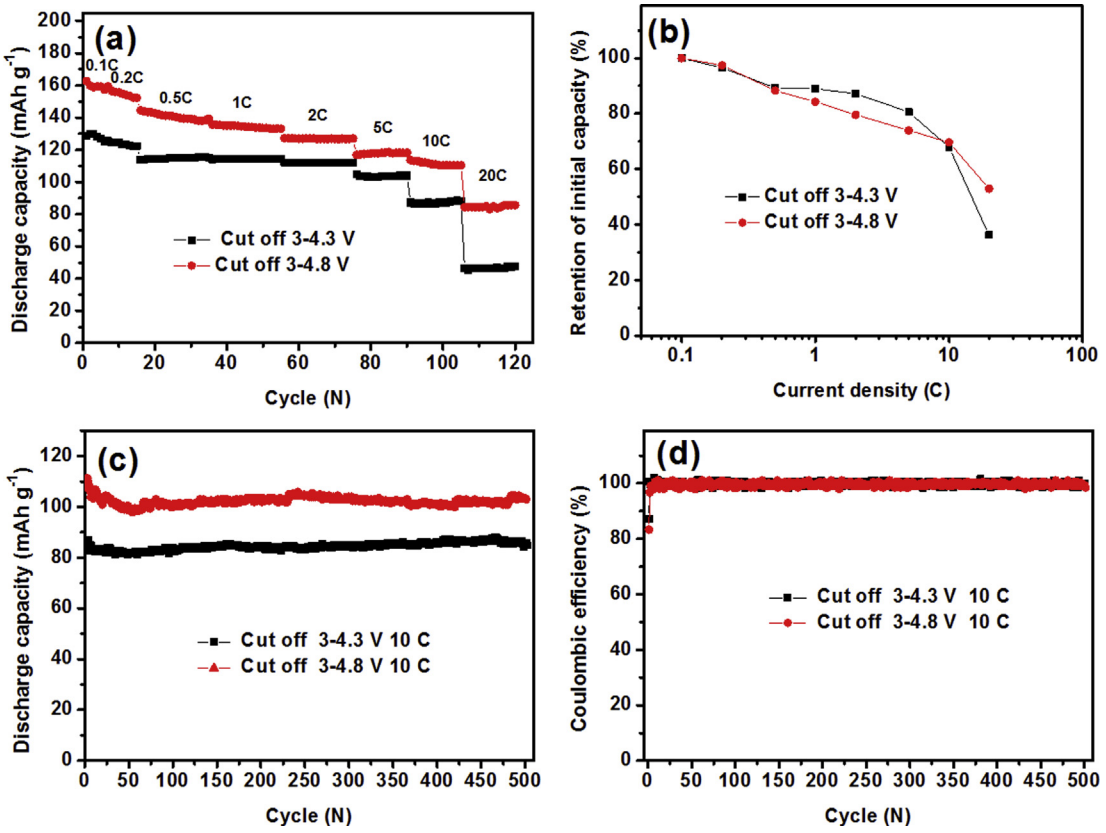

Fig. 5. (a) Rate performance of $Li_3V_2(PO_4)_3$/C electrodes; (b) capacity retention with respect to initial capacity at C/10 at various current densities; (c) cycling performance of $Li_3V_2(PO_4)_3$/C, with (d) coulombic efficiency at 10C. (1C = 197 mAh g^{-1} for both voltage ranges, and the electrolyte is 1 M $LiPF_6$ in a 1:2 (v/v) mixture of ethylene carbonate (EC) and diethyl carbonate (DEC).).

size ranging from 0.5 to 1.5 mm. The prepared sample of $Li_3V_2(PO_4)_3$/C delivered a reversible discharge capacity of 100 mAh g^{-1} after 100 cycles at 20 C in the voltage range of 3.0–4.3 V (1C = 133 mAh g^{-1}), exhibiting excellent rate capability and cycling performance. The cell retains 90% of initial discharge capacity after 100 cycles at 20 C, but there was no report on long term testing of $Li_3V_2(PO_4)_3$/C in the voltage range of 3.0–4.8 V.

The cyclic voltammetry (CV) technique is widely employed to estimate the Li^+ diffusion coefficient [18,34,35,40]. Fig. 6(a) shows the CV curves of $Li_3V_2(PO_4)_3$/C at various scan rates in the voltage range of 3.0–4.3 V: the peaks of a/a′, b/b′, and c/c′ correspond to the 0.5, 0.5, and 1 Li extraction–insertion, respectively. Fig. 6(b) presents fitted line plots of the peak current (i_p) of the CV as a function of the square root of the scan rate ($v^{1/2}$), indicating diffusion-controlled behaviour. The diffusion coefficient of Li^+ could be calculated based on Equations (3) and (4), expressed as

$$i_p = 2.69 \times 10^5 n^{3/2} A D^{1/2} v^{1/2} C_0^* \quad (3)$$

$$D = \left(i_p/v^{1/2}\right) \Big/ \left(2.69 \times 10^5 n^{3/2} A C_0^*\right) = \left[k/\left(2.69 \times 10^5 n^{3/2} A C_0^*\right)\right]^2 \quad (4)$$

where k is the slope of the linear fit of the peak current i_p as a function of the square root of the scan rate ($v^{1/2}$), n is the number of electrons per reaction species, A is the surface area of the electrode (cm^2), D is the diffusion coefficient of Li^+ ($cm^2\ s^{-1}$), C_0^* is the concentration of lithium ions corresponding to the different specific electrochemical reaction steps (mol cm^{-3}). For the Li^+ diffusion in the electrode, C_0^* is calculated as 3.687×10^{-3} mol cm^{-3} [34] ($C_0^* = (2Li/6.02 \times 10^{23})$ mol/$(900.927 \times 10^{-24})$ cm^3), the number of Li ions per unit cell divided by the volume of the cell (900.927(3) Å^3). Therefore, the values for the Li^+ diffusion coefficient D in the solid state electrode and the electrolyte have been calculated according to Equation. (2) and are listed in Table 1. The Li ion diffusion coefficient of the $Li_3V_2(PO_4)_3$/C is calculated to be on the order of $\sim 10^{-9}$ $cm^2\ s^{-1}$, which is very close to the results of Liu et al. [35], which represent excellent cycling performance for their carbon coated-$Li_3V_2(PO_4)_3$ and nanocomposite $Li_3V_2(PO_4)_3$/graphene. Therefore, the 3D network structure of $Li_3V_2(PO_4)_3$/C shows good kinetic properties for lithium diffusion during the charge/discharge processes, leading to its excellent rate capabilities and cycling performance.

Table 1
The calculated lithium diffusion coefficients for $Li_3V_2(PO_4)_3$/C at scan rates from 0.05 to 0.25 mV s^{-1}.

$Li_3V_2(PO_4)_3$/C	Peak	D (10^{-9} $cm^2\ s^{-1}$)
Oxidation (charge)	c	7.00
	b	7.50
	a	6.09
Reduction (discharge)	c′	5.38
	b′	4.06
	a′	2.68

The degradation of conventional electrolytes ($LiPF_6$ in ethylene carbonate (EC): diethyl carbonate (DEC), EC: dimethyl carbonate (DMC), etc.) at high working voltage (>4.6 V) is one of the major difficulties for the practical application of $Li_3V_2(PO_4)_3$/C. Recently, the high anodic stability (>5 V), relatively high ionic conductivity, and non-flammability of pyrrolidinium bis(trifluoromethanesulfonyl) amide salt based ionic liquids (ILs) (1 M $LiNTf_2$ in [C_4mpyr][NTf_2] and [C_3mpyr][NTf_2]) have led to good electrochemical properties in battery tests [23–25]. The electrochemical window of stability is in excess of 5.5 V [23,24]. Therefore, the electrochemical performances of $Li_3V_2(PO_4)_3$/C measured with conventional electrolyte (1 M $LiPF_6$ in EC: DEC) and with ILs (1 M $LiNTf_2$ in [C_4mpyr]

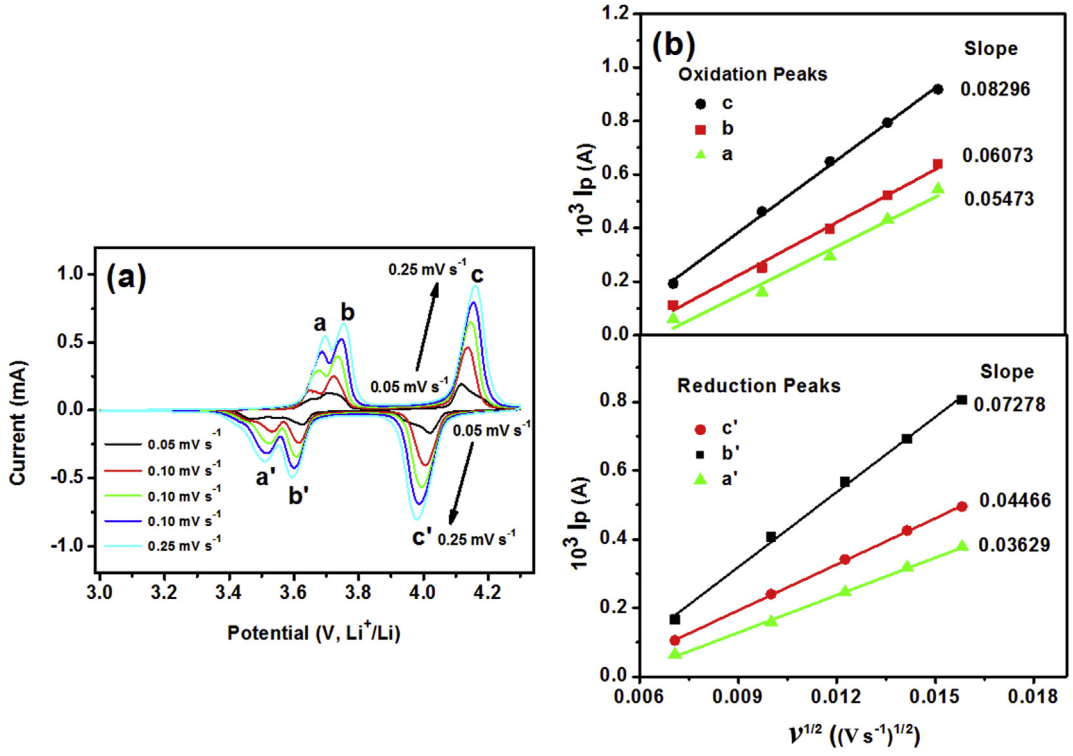

Fig. 6. (a) Cyclic voltammograms of $Li_3V_2(PO_4)_3$/C at different scan rates from 0.05 to 0.25 mV s^{-1}. (b) Linear fits of the peak current i_p for the oxidation and reduction peaks as functions of the square root of the scan rate $v^{1/2}$. (The electrolyte was 1 M $LiPF_6$ in a 1:2 (v/v) mixture of ethylene carbonate (EC) and diethyl carbonate (DEC).).

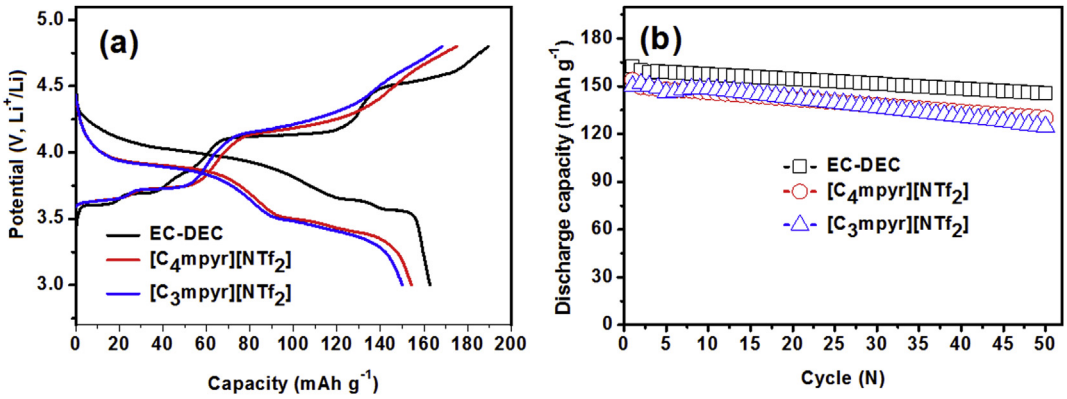

Fig. 7. (a) Initial charge/discharge profiles and (b) cycling performances of $Li_3V_2(PO_4)_3$ electrodes measured with different electrolytes at the 0.1C rate in the voltage range of 3.0–4.8 V at room temperature.

$[NTf_2]$ and $[C_3mpyr][NTf_2]$) are compared in Fig. 7. Fig. 7(a) shows the initial charge–discharge profiles obtained with the $Li_3V_2(PO_4)_3$/C electrode in the conventional and IL electrolytes at the 0.1C rate in the voltage range of 3.0–4.8 V at room temperature. The $Li_3V_2(PO_4)_3$/C delivered higher discharge capacity in conventional electrolyte, 162.3 mAh g^{-1}, than in the ionic liquids, 153.9 mAh g^{-1} and 150.1 mAh g^{-1} for $[C_4mpyr][NTf_2]$ and $[C_3mpyr][NTf_2]$ electrolytes, respectively. The $Li_3V_2(PO_4)_3$/C shows lower initial irreversible capacity, however, in 1 M $LiNTf_2$ in $[C_4mpyr][NTf_2]$ and $[C_3mpyr][NTf_2]$ electrolytes, 26.9 mAh g^{-1} and 28.2 mAh g^{-1}, respectively, compared to that in conventional electrolyte, 32.8 mAh g^{-1}. The low initial irreversible capacity indicates the highly reversible nature of the reaction for $Li_3V_2(PO_4)_3$ cycled in the IL electrolytes with 1 M $LiNTf_2$ in $[C_4mpyr][NTf_2]$ and $[C_3mpyr][NTf_2]$. The cycling performances of the $Li_3V_2(PO_4)_3$/C electrodes measured in the conventional and IL electrolytes are shown in Fig. 7(b). The retained discharge capacities at the 50th cycle for $Li_3V_2(PO_4)_3$ were 145.6 mAh g^{-1}, 130.1 mAh g^{-1}, and 124.7 mAh g^{-1}, with 89.7%, 84.5%, and 83.1% capacity retention in the conventional electrolyte, and the $[C_3mpyr][NTf_2]$ and $[C_4mpyr][NTf_2]$ electrolytes, respectively. Compared to the conventional electrolyte, the ILs are associated with lower discharge capacity and retention of initial capacity, which should probably be attributed to the higher viscosity and unstable SEI layer in ILs.

4. Conclusions

A three-dimensional (3D) network $Li_3V_2(PO_4)_3$/C cathode material for lithium ion batteries was synthesized by the highly efficient and low-cost microwave assisted hydrothermal method, followed by a post-annealing process. The synchrotron powder X-ray diffraction analysis results, as well as those from scanning electron microscopy and transmission electron microscopy, confirmed that the single-phase $Li_3V_2(PO_4)_3$ with monoclinic structure was composed of nanowires and microsized particles. Electrochemical results showed that the $Li_3V_2(PO_4)_3$/C electrode measured at 10 C after 500 cycles could still deliver discharge capacities of 85.4 mAh g^{-1} and 103.4 mAh g^{-1}, with capacity retention of 99.3% and 95.9%, in the 3.0–4.3 V and 3.0–4.8 V voltage ranges, respectively, indicating excellent cycling performance. Furthermore, the $Li_3V_2(PO_4)_3$/C can be cycled at 0.1C in the voltage range of 3.0–4.8 V in the green, high anodic stability, non-flammable ILs. Compared to conventional electrolyte, ILs have lower discharge capacity and retention of initial capacity, which should probably be attributed to the higher viscosity of $[C_4mpyr][NTf_2]$ and $[C_4mpyr][NTf_2]$, reducing the amount of ions and electrons shuttling between the $Li_3V_2(PO_4)_3$/C and the ILs. The relatively acceptable electrochemical performance in the ILs, however, make the ILs a good choice to address the problems of electrolyte degradation associated with high voltage cathodes (>4.6 V) and increase the operating safety of lithium ion batteries.

Acknowledgements

Financial support was provided by the Australian Research Council through a Discovery project (DP110103909). The authors thank Dr. T. Silver for critical reading of the manuscript.

References

[1] A.K. Padhi, K.S. Nanjundaswamy, J.B. Goodenough, J. Electrochem. Soc. 144 (1997) 1188–1194.
[2] M.K. Devaraju, I. Honma, Adv. Energy Mater. 2 (2012) 284–297.
[3] J.-K. Kim, C.-R. Shin, J.-H. Ahn, A. Matic, P. Jacobsson, Electrochem. Commun. 13 (2011) 1105–1108.
[4] H. Huang, S.C. Yin, T. Kerr, N. Taylor, L.F. Nazar, Adv. Mater. 14 (2002) 1525–1528.
[5] M.Y. Saidi, J. Barker, H. Huang, J.L. Swoyer, G. Adamson, J. Power Sources 119 (2003) 266–272.
[6] M.M. Ren, Z. Zhou, L.W. Su, X.P. Gao, J. Power Sources 189 (2009) 786–789.
[7] L. Wang, L.B. Yang, L. Gong, X.Q. Jiang, K. Yuan, Z.B. Hu, Electrochim. Acta 56 (2011) 6906–6911.
[8] J. Xu, Y. Zhao, Q. Kuang, Y. Dong, Electrochim. Acta 56 (2011) 6562–6567.
[9] Q. Kuang, Y. Zhao, J. Xu, J. Phys. Chem. C 115 (2011) 8422–8429.
[10] L. Adam, A. Guesdon, B. Raveau, J. Solid State Chem. 181 (2008) 3110–3115.
[11] S.-i. Nishimura, M. Nakamura, R. Natsui, A. Yamada, J. Am. Chem. Soc. 132 (2010) 13596–13597.
[12] H. Kim, I. Park, D.-H. Seo, S. Lee, S.-W. Kim, W.J. Kwon, Y.-U. Park, C.S. Kim, S. Jeon, K. Kang, J. Am. Chem. Soc. 134 (2012) 10369–10372.
[13] R.A. Shakoor, H. Kim, W. Cho, S.Y. Lim, H. Song, J.W. Lee, J.K. Kang, Y.-T. Kim, Y. Jung, J.W. Choi, J. Am. Chem. Soc. 134 (2012) 11740–11748.
[14] K. Trad, D. Carlier, L. Croguennec, A. Wattiaux, B. Lajmi, M. Ben Amara, C. Delmas, J. Phys. Chem. C 114 (2010) 10034–10044.
[15] L. Dimesso, C. Forster, W. Jaegermann, J.P. Khanderi, H. Tempel, A. Popp, J. Engstler, J.J. Schneider, A. Sarapulova, D. Mikhailova, L.A. Schmitt, S. Oswald, H. Ehrenberg, Chem. Soc. Rev. 41 (2012) 5068–5080.
[16] Q.Q. Chen, T.T. Zhang, X.C. Qiao, D.Q. Li, J.W. Yang, J. Power Sources 234 (2013) 197–200.
[17] H.W. Liu, C.X. Cheng, X.T. Huang, J.L. Li, Electrochim. Acta 55 (2010) 8461–8465.
[18] Y.Q. Qiao, X.L. Wang, Y.J. Mai, J.Y. Xiang, D. Zhang, C.D. Gu, J.P. Tu, J. Power Sources 196 (2011) 8706–8709.
[19] A.Q. Pan, D.W. Choi, J.G. Zhang, S.Q. Liang, G.Z. Cao, Z.M. Nie, B.W. Arey, J. Liu, J. Power Sources 196 (2011) 3646–3649.
[20] X.H. Rui, D.H. Sim, K.M. Wong, J.X. Zhu, W.L. Liu, C. Xu, H.T. Tan, N. Xiao, H.H. Hng, T.M. Lim, Q.Y. Yan, J. Power Sources 214 (2012) 171–177.
[21] L. Zhang, H. Xiang, Z. Li, H. Wang, J. Power Sources 203 (2012) 121–125.
[22] S. Lee, Y. Cho, H.-K. Song, K.T. Lee, J. Cho, Angew. Chem. Int. Ed. 51 (2012) 8748–8752.
[23] D.R. MacFarlane, P. Meakin, J. Sun, N. Amini, M. Forsyth, J. Phys. Chem. B 103 (1999) 4164–4170.
[24] P.C. Howlett, N. Brack, A.F. Hollenkamp, M. Forsyth, D.R. MacFarlane, J. Electrochem. Soc. 153 (2006) A595.

[25] J.T. Xu, S.L. Chou, M. Avdeev, M. Sale, H.K. Liu, S.X. Dou, Electrochim. Acta 88 (2013) 865–870.
[26] C.W. Sun, S. Rajasekhara, Y.Z. Dong, J.B. Goodenough, ACS Appl. Mater. Interfaces 3 (2011) 3772–3776.
[27] C.X. Chang, J.F. Xiang, X.X. Shi, X.Y. Han, L.J. Yuan, J.T. Sun, Electrochim. Acta 54 (2008) 623–627.
[28] Y.Q. Qiao, J.P. Tu, J.Y. Xiang, X.L. Wang, Y.J. Mai, D. Zhang, W.L. Liu, Electrochim. Acta 56 (2011) 4139–4145.
[29] F. Teng, Z.H. Hu, X.H. Ma, L.C. Zhang, C.X. Ding, Y. Yu, C.H. Chen, Electrochim. Acta 91 (2013) 43–49.
[30] G. Yang, H.D. Liu, H.M. Ji, Z.Z. Chen, X.F. Jiang, J. Power Sources 195 (2010) 5374–5378.
[31] J. Yan, W.F. Mao, H. Xie, Z.Y. Tang, W. Yuan, X.C. Chen, Q. Xu, L. Ma, Mater. Res. Bull. 47 (2012) 1609–1612.
[32] B. Toby, J. Appl. Crystallogr. 34 (2001) 210–213.
[33] Y.H. Chen, Y.M. Zhao, X.N. An, J.M. Liu, Y.Z. Dong, L. Chen, Electrochim. Acta 54 (2009) 5844–5850.
[34] X.H. Rui, N. Ding, J. Liu, C. Li, C.H. Chen, Electrochim. Acta 55 (2010) 2384–2390.
[35] H.D. Liu, G. Yang, X.F. Zhang, P. Gao, L. Wang, J.H. Fang, J. Pinto, X.F. Jiang, J. Mater. Chem. 22 (2012) 11039–11047.
[36] A.R. Cho, J.N. Son, V. Aravindan, H. Kim, K.S. Kang, W.S. Yoon, W.S. Kim, Y.S. Lee, J. Mater. Chem. 22 (2012) 6556–6560.
[37] T. Zhu, J.S. Chen, X.W. Lou, J. Phys. Chem. C 115 (2011) 9814–9820.
[38] Q. Kuang, Y.M. Zhao, X.N. An, J.M. Liu, Y.Z. Dong, L. Chen, Electrochim. Acta 55 (2010) 1575–1581.
[39] W.-f. Mao, J. Yan, H. Xie, Y. Wu, Z.-y. Tang, Q. Xu, Mater. Res. Bull. 47 (2012) 4527–4530.
[40] J. Su, X.-L. Wu, J.-S. Lee, J. Kim, Y.-G. Guo, J. Mater. Chem. A 1 (2013) 2508–2514.